Int. J. Econ. Environ. Geol., Vol. 17, Issue 2, 2026, 89-102 doi:10.46660/int.j.econ.environ.geol.v17i2.840.
Journal home page: www.econ-environ-geol.org

GEOCHEMICAL AND PETROGENETIC DISCRIMINATION OF PRODUCTIVE AND BARREN PEGMATITES IN THE KOHISTAN LADAKH ISLAND ARC (KLIA), NORTHERN PAKISTAN

JOHAR ALI[1]*, KAMARAN SIDDIQUE[2]
[1]Department of Earth Sciences, School of Science, Shiraz University, Iran
[2]Institute of Geology, University of Azad Jammu and Kashmir, Muzaffarabad

Received: *15 May, 2026* ***Accepted:*** *28 June, 2026*

Abstract: Granitic pegmatites are major repositories of critical metals, including Li, Be, Nb, Ta, Cs, and Sn, yet distinguishing fertile from barren pegmatites remains a major challenge in complex arc-related terranes. This study investigates the petrogenesis and fertility of pegmatites from the Gilgit Formation and the Nyit Bruk Bisil district of the Shigar Valley within the Kohistan, Ladakh Island Arc (KLIA), and northern Pakistan. Integrated field observations, petrography, and whole-rock geochemical analyses (XRF and ICP-OES) were used to evaluate magmatic evolution and rare-metal mineralization. Pegmatites are structurally controlled, emplaced along shear zones, lithological contacts, and late-stage fractures within granitoid, meta-sedimentary host rocks. Petrographic observations reveal internally zoned pegmatites composed predominantly of quartz, feldspar, mica, and accessory rare-element minerals. Geochemical data indicate strongly peraluminous, highly fractionated melts enriched in incompatible elements (Li, Rb, Cs, Nb, Ta, and Sn), and particularly in spodumene-bearing pegmatites relative to barren granitoid-related bodies. Diagnostic elemental ratios (Rb vs. Sr, K vs. Rb, Nb vs. Ta, and Cs vs. Rb) effectively distinguish fertile from barren pegmatites and record progressive magmatic differentiation and late-stage fluid melt interaction. Trace-element relationships, including Li, Rb and Ta, Be systematics, further support an evolutionary trend characteristic of Li, Cs and Ta (LCT) pegmatites. These results indicate that fertile pegmatites within the KLIA originated from highly evolved peraluminous granitoid melts subsequently modified by volatile-rich magmatic fluids. Pegmatite fertility is therefore governed by advanced melt fractionation, structural focusing of residual melts, and spatial association with evolved granitoid sources. This study provides a detailed geochemical framework for rare-metal exploration and advanced understanding of pegmatite metallogenesis in arc-related tectonic settings.

Keywords: Granitic pegmatites, rare metals, geochemistry, Gilgit Formation, metallogenesis.

Introduction

Granitic pegmatites constitute one of the most important hosts of rare-metal mineralization, including Li, Be, Nb, Ta, Cs, and Sn, and are therefore central to critical-metal resource exploration (London, 2018; Wang *et al*., 2023). The distinction between productive (fertile) and barren pegmatites is fundamental for understanding their petrogenesis and for guiding exploration strategies in orogenic and arc-related terranes (Cerny, 1991; Bell & Bomgaars, 2015). Recent advances in geochemical and isotopic approaches have significantly enhanced the ability to discriminate fertile pegmatites, particularly through the application of trace element ratios (e.g., Rb vs. Sr, Nb vs. Ta, Cs vs. Rb) and rare-metal enrichment signatures, which are closely linked to specific melt evolution processes (Wang *et al*., 2023; Smith *et al*., 2024).

The Kohistan, Ladakh Island Arc (KLIA) in northern Pakistan provides an exceptional natural laboratory for investigating pegmatite fertility within a convergent arc setting formed between the Indian and Eurasian plates. Developed during Neo-Tethyan subduction and subsequent continental collision, the (KLIA) preserves a well-exposed arc sequence comprising abundant granitoids and associated pegmatites (Ahmad *et al*., 2025). Within this arc system, the Gilgit Formation and the Nyit-Bruk–Bisil area of the Shigar district host a diverse assemblage of pegmatitic bodies, ranging from simple quartz, feldspar veins to complex rare-metal-enriched systems. These pegmatites exhibit substantial variability in mineralogy, geochemistry, and fertility, although the controlling factors governing this variability remain poorly constrained.

While previous regional studies have established the broader geological framework and plutonic evolution of the KLIA (Searle *et al*., 2020; Ahmad *et al*., 2025), there remains a critical need for integrated field investigations coupled with high-precision geochemical analyses (XRF, AAS and ICP-OES) to effectively discriminate between fertile and barren pegmatites. Such an integrated approach provides detailed information on magmatic differentiation, trace element partitioning, and melt–fluid evolution, thereby refining genetic models of pegmatite formation and enhancing

*Corresponding author e-mail: jgeologist19@gmail.com

exploration strategies in complex arc environments (Wang *et al*., 2023; Smith *et al*., 2024).

Geological Setting

The study area is situated in the northern Kohistan Ladakh Island Arc (KLIA) of northern Pakistan, a Late Cretaceous intra-oceanic arc developed within the Neo-Tethys during convergence between the Indian and Eurasian plates. The KLIA is bounded by the Main Mantle Thrust (MMT) to the south and the Main Karakoram Thrust (MKT) to the north, separating it from the Indian and Karakoram continental domains, respectively (Fig. 1). The arc preserves a long-lived record of subduction-related magmatism, crustal differentiation, arc continent collision, metamorphism, and subsequent exhumation (Jagoutz & Behn, 2013).

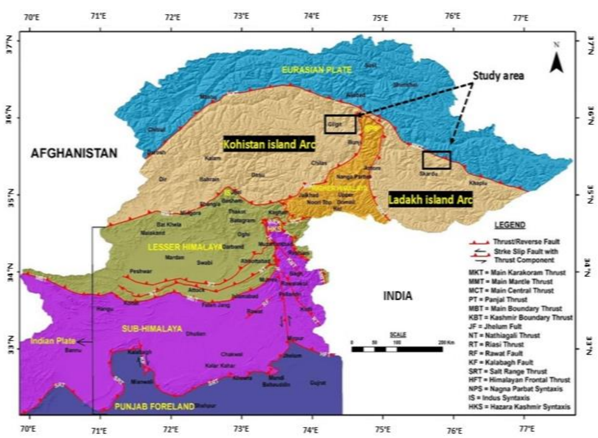

Fig. 1 Regional tectonic framework of northern Pakistan showing the principal lithotectonic domains, major thrusts, and sutures of the Himalayan, Karakoram orogen (after Wadia, 1931; Searle & Khan, 1996; Khan *et al*., 2016).

These processes generated extensive intermediate to felsic plutonism and highly evolved late-stage melts that provided favorable conditions for pegmatite formation. In the study region, the Gilgit Formation of the Jaglot Group constitutes an important country-rock sequence and comprises amphibolite- to granulite-facies metasedimentary and metavolcanic rocks intruded by dioritic to granodioritic plutons (Burg *et al*., 2022). The formation provides structurally favorable sites for the emplacement of late-stage felsic melts. Pegmatites occur principally along fractures, shear zones, and lithological contacts, where evolved granitic melts accumulated during the final stages of magmatic crystallization.

Their mineralogical and geochemical variability, including both barren and rare-element-enriched bodies, reflects progressive magmatic differentiation, incompatible-element concentration, and structurally controlled melt migration (London, 2008, 2018; Wang *et al*., 2023). The broader study area extends along the Indus River between Dassu and Skardu, adjacent to the MKT, which marks the boundary between the Karakoram Block and the KLIA (Fig. 2). The local geology comprises granodioritic and gneissic rocks, metamafic rocks, marble, serpentinite, pegmatites, and Quaternary deposits, including the Katzarah, Bauma Harel, Burji La, Daltumbore, and Dassu Gneiss units (Hanson, 1988, 1989).

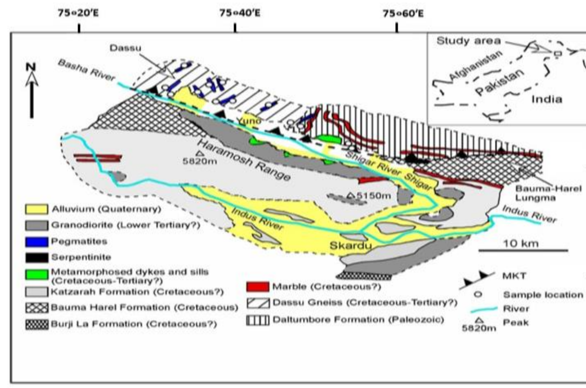

Fig. 2 Simplified geological map of the study region between Dassu and Skardu, northern Pakistan, showing the distribution of major lithological units and the Main Karakoram Thrust (after Hanson, 1988, 1989).

Pegmatites contain quartz, feldspar, mica, garnet, tourmaline, and locally aquamarine, indicating crystallization from highly evolved felsic melts. Their spatial association with fractures, shear zones, and lithological contacts suggests that structural permeability played an important role in melt emplacement and localization. Collectively, the lithological and structural relationships record the transition from arc-related magmatism to collision-related crustal reworking and exhumation, providing the geological framework for the generation, differentiation, and emplacement of rare-element pegmatites in the region (Palin *et al*., 2018).

Materials and Methods

A total of 189 pegmatite samples collected from the Gilgit Formation and the Nyit–Bruk–Bisil pegmatite fields of the Shigar Valley were subjected to whole-rock geochemical analysis. Major element oxides (n = 150) were determined using X-ray fluorescence spectrometry (XRF) on fused glass beads following lithium tetraborate fusion procedures. Trace element concentrations, including Li, Rb, Cs, Nb, Ta, and Sn (n=39), were analyzed by inductively coupled plasma optical emission spectrometry (ICP–OES) after complete four-acid digestion (HF, HNO_3, $HClO_4$, HCl). Gold (Au) and silver (Ag) concentrations were determined using atomic absorption spectrometry (AAS) following aqua regia and multi-acid digestion protocols, depending on sample composition and detection requirements (Table 1).

Analytical measurements were carried out using calibrated laboratory instrumentation operating under ISO/IEC 17025-accredited analytical procedures. Quality assurance and quality control (QA/QC) protocols included the routine

Table 1. Whole-rock geochemistry of GP and SP samples (ppm) showing major, trace, and REE variations.

Sample	GP-1	GP-2	GP-3	GP-4	GP-5	GP-6	GP-7	GP-8	GP-9	GP-10	GP-11	GP-12	GP-13	GP-14	GP-15
$SiO_{2\ (wt.\%)}$	67.681	73.386	78.724	80.546	7.816	8.021	77.09	58.17	84.673	66.606	44.961	40.18	45.137	77.426	90.797
Al_2O_3	11.978	12.554	14.791	14.409	1.403	1.646	17.386	14.851	12.763	19.825	15.667	16.495	19.168	15.684	5.646
$Fe_2O_{3\ (total)}$	7.829	0.362	0.562	0.482	0.381	0.419	0.387	8.868	0.306	6.272	15.551	19.762	16.185	0.626	1.056
MgO	bdl	5.986	2.192	1.941	6.906	3.015	bdl	6.929	bdl	bdl	15.322	bdl	14.361	4.288	bdl
CaO	11.064	7.558	2.951	1.953	82.989	86.054	4.894	10.37	2.073	5.658	6.976	21.477	3.697	1.627	2.055
TiO_2	0.842	0.109	0.652	0.598	0.433	0.777	0.195	0.556	0.153	1.516	1.327	1.248	1.028	0.253	0.416
MnO	0.396	0.045	0.054	0.018	0.072	0.068	0.048	0.2	0.032	0.122	0.196	0.283	0.238	0.037	0.029
P_2O_5	0.211	bdl	0.075	0.051	bdl	bdl	bdl	0.056	bdl	bdl	bdl	0.556	0.187	0.058	bdl
LE (ppm)	573392	554379	593814	639983	542161	537976	656042	581271	592233	612938	533095	544521	537815	538535	610092
S	1185	1923	2234	1163	170	506	2811	1600	1396	1015	1324	14723	22500	2813	6763
V	bdl	bdl	328	bdl	351	bdl	bdl	bdl	bdl	bdl	316	198	bdl	bdl	bdl
Cr	bdl	bdl	bdl	79	bdl	bdl	bdl	443	bdl	bdl	bdl	bdl	618	bdl	bdl
Co	611	bdl	bdl	186	bdl	bdl	bdl	181	bdl	bdl	bdl	1047	bdl	bdl	181
Ni	bdl	62	bdl	bdl	27	64	72	229	25	54	337	bdl	141	71	bdl
Cu	8086	77	85	49	21	bdl	76	4119	57	37	72	84	138	36	23
Zn	44	58	51	19	68	23	18	147	bdl	54	108	110	155	25	bdl
As	bdl	10	bdl	bdl	bdl	bdl	8	20	bdl	12	bdl	bdl	33	bdl	16
Se	9	6	11	10	4	6	11	16	13	7	bdl	4	22	10	11
Rb	10	5	242	184	14	11	30	45	157	68	85	22	12	128	19
Sr	206	225	116	152	217	201	289	356	92	1128	321	2120	295	200	227
Y	117	23	12	15	31	25	22	35	34	16	44	53	40	11	28
Zr	45	128	80	53	39	47	88	66	123	84	74	90	69	86	65
Nb	54	25	15	29	42	17	26	33	20	25	40	55	33	37	29
Mo	54	25	42	40	56	63	32	34	30	62	83	86	50	46	37
Ag	59	34	50	17	63	27	13	57	14	39	53	21	20	23	46
Cd	51	bdl	137	54	236	bdl	116	161	170	128	334	66	203	115	85
Sn	258	140	85	135	144	231	132	bdl	75	bdl	317	138	111	187	bdl
Sb	313	214	178	129	280	176	59	100	138	302	570	272	112	172	172
Ba	408	531	322	381	512	488	610	968	272	1076	803	460	751	907	511
La	687	1001	665	391	724	690	778	544	865	682	1654	548	709	1455	1074
Ce	952	990	444	595	747	887	745	780	321	653	1030	1066	1457	1659	1068
Pr	2090	1283	1014	1271	1600	2160	839	1912	1284	548	2334	1106	2026	1146	960
Nd	2325	1314	950	2552	1688	2640	1830	2664	1413	1910	4172	3259	3226	2228	1496
W	70	42	bdl	54	bdl	59	29	bdl	48	55	50	62	29	14	65
Pb	bdl	bdl	42	68	14	bdl	8	bdl	33	bdl	bdl	33	bdl	27	bdl
Bi	72	41	61	44	89	82	55	126	75	124	217	101	60	86	44

Table 1 continued…

Sample	GP-16	GP-17	GP-18	GP-19	GP-20	GP-21	GP-22	GP-23	GP-24	GP-25	GP-26	GP-27	GP-28	GP-29	GP-30
$SiO_{2\ (wt.\%)}$	78.68	67.031	70.275	81.351	99.783	92.667	60.495	81.19	53.027	43.933	49.117	68.214	71.964	81.534	97.189
Al_2O_3	15.175	24.77	22.176	15.408	bdl	5.594	28.134	9.728	13.966	24.92	22.618	8.725	10.709	15.804	2.251
$Fe_2O_{3\ (total)}$	1.925	0.337	1.353	0.328	0.054	0.287	3.866	6.387	14.518	5.832	13.097	16.444	9.872	0.389	0.15
MgO	bdl	bdl	bdl	bdl	bdl	bdl	bdl	bdl	11.892	bdl	5.558	3.528	3.606	bdl	bdl
CaO	3.657	7.233	5.621	2.25	bdl	1.392	6.444	1.916	4.812	24.13	8.286	1.998	2.609	1.996	0.294
TiO_2	0.368	0.577	0.394	0.505	0.127	bdl	0.991	0.744	1.361	1.023	0.944	0.994	1.067	0.255	0.102
MnO	0.069	0.053	0.093	0.073	0.036	0.06	0.069	0.035	0.352	0.162	0.082	0.097	0.132	0.022	0.015
P_2O_5	0.126	bdl	0.086	0.085	bdl	bdl	bdl	bdl	0.071	bdl	0.298	bdl	0.04	bdl	bdl
LE	639682	653578	621051	660689	516305	655417	539643	538206	560527	504042	545041	727823	381877	577674	561322
S	3190	2147	1714	2344	915	1485	648	14003	77336	2000	73281	17198	1425	1467	1708
V	222	293	bdl	bdl	219	bdl	242	bdl	328	bdl	bdl	bdl	bdl	bdl	bdl
Cr	bdl	208	bdl	bdl	bdl	85	bdl	bdl	316	bdl	bdl	bdl	239	bdl	bdl
Co	bdl	54	100	79	70	bdl	bdl	bdl	bdl	335	507	bdl	402	32	bdl
Ni	51	33	41	42	bdl	bdl	19	bdl	64	75	74	25	177	bdl	20
Cu	41	70	32	22	51	37	24	26	125	39	191	214	179	72	60
Zn	21	36	22	36	23	19	16	24	115	39	51	37	218	27	9
As	12	bdl	bdl	bdl	bdl	bdl	5	bdl	bdl	18	bdl	bdl	bdl	bdl	bdl
Se	9	5	6	13	9	12	5	10	7	18	11	6	8	8	6
Rb	26	12	13	63	9	11	30	32	10	21	51	17	193	64	40
Sr	552	972	876	346	11	199	1854	180	299	986	244	69	291	301	87
Y	15	11	20	18	10	52	24	28	44	31	41	19	28	17	28
Zr	48	39	62	19	23	31	118	100	80	1055	81	51	52	44	31
Nb	21	29	12	12	19	15	21	30	8	35	11	27	39	27	29
Mo	34	40	24	42	18	25	12	27	48	41	45	37	52	32	26
Ag	12	29	40	13	20	45	24	47	55	39	60	51	59	22	35
Cd	223	141	106	31	83	108	48	105	80	274	187	117	97	202	146
Sn	bdl	194	91	129	113	121	bdl	225	115	105	172	bdl	134	103	124
Sb	77	245	161	174	72	161	206	234	132	143	301	216	368	171	91
Ba	680	534	833	994	240	428	565	727	362	591	867	508	1682	468	640
La	1201	903	505	1050	938	1334	845	864	1038	507	1362	845	1011	549	826
Ce	1707	764	768	961	839	1875	763	1717	1346	729	865	560	1174	1029	1003
Pr	1161	1329	1180	1071	1129	1307	1549	1259	1764	1420	1757	1192	1656	1340	911
Nd	2708	1511	1835	1959	2448	2957	3429	2941	4008	3047	1582	1365	2625	2300	2416
W	16	bdl	bdl	bdl	33	15	45	50	31	95	54	58	59	bdl	34
Pb	bdl	16	bdl	23	bdl	bdl	bdl	9	bdl	bdl	bdl	bdl	bdl	bdl	bdl
Bi	67	57	154	40	24	97	35	bdl	80	bdl	49	93	bdl	49	47

Continued….

Table 1 continued…

Sample	GP-31	GP-32	GP-33	GP-34	GP-35	GP-36	GP-37	GP-38	GP-39	GP-40	GP-41	GP-42	GP-43	GP-44	GP-45
$SiO_{2\ (wt.\%)}$	51.144	78.76	83.759	76.462	80.221	84.891	75.604	73.478	55.497	79.313	53.421	80.777	89.952	74.409	84.196
Al_2O_3	14.562	17.228	13.923	19.81	16.177	10.706	16.286	21.408	18.189	17.929	19.601	16.326	8.23	21.344	12.976
$Fe_2O_{3\ (total)}$	23.117	0.338	0.104	0.286	0.325	0.49	2.989	0.514	14.573	0.919	23.344	0.948	0.205	2.246	0.663
MgO	7.531	bdl	bdl	bdl	bdl	bdl	bdl	bdl	8.1	bdl	bdl	bdl	bdl	bdl	bdl
CaO	1.065	3.431	1.966	3.104	2.801	3.548	4.524	4.096	2.157	1.546	1.965	1.281	1.455	1.262	1.649
TiO_2	2.052	0.203	0.219	0.264	0.428	0.241	0.534	0.415	1.262	0.252	1.579	0.111	0.106	0.466	0.322
MnO	0.528	0.041	0.029	0.074	0.048	0.025	0.062	0.088	0.135	0.041	0.091	0.557	0.053	0.273	0.194
P_2O_5	bdl	bdl	bdl	bdl	bdl	0.1	bdl	bdl	0.087	bdl	bdl	bdl	bdl	bdl	bdl
LE	413297	602828	643468	593527	562407	530728	526089	636951	496707	561798	647635	532071	596916	639865	586597
S	1443	1099	1789	766	1276	1339	1293	1543	15887	1552	32521	1882	1391	1309	1318
V	319	bdl	bdl	bdl	bdl	bdl	206	bdl	468	bdl	bdl	138	113	160	bdl
Cr	bdl	bdl	bdl	bdl	bdl	97	bdl	bdl	bdl	75	420	bdl	bdl	bdl	168
Co	655	bdl	51	bdl	49	142	bdl	89	334	bdl	bdl	bdl	bdl	bdl	52
Ni	bdl	25	bdl	bdl	26	bdl	25	33	92	28	43	bdl	30	34	14
Cu	169	13	65	45	48	55	35	70	1197	90	943	32	32	40	56
Zn	1128	6	bdl	38	25	9	62	17	261	26	325	65	40	99	63
As	22	bdl	4	18	bdl	bdl	bdl	6	bdl	7	bdl	6	bdl	bdl	8
Se	26	6	5	8	7	6	13	10	7	2	17	3	7	10	9
Rb	1486	12	19	21	25	16	45	13	79	132	39	272	171	189	34
Sr	27	354	170	188	366	577	659	287	85	312	328	81	31	27	132
Y	31	27	21	20	26	17	23	14	21	6	27	56	36	54	41
Zr	32	42	116	31	27	49	51	33	39	35	98	54	45	68	47
Nb	812	26	27	29	17	16	26	23	43	44	29	40	30	67	26
Mo	46	43	25	18	25	45	54	26	42	34	31	40	22	30	49
Ag	25	55	6	31	31	30	42	17	45	26	56	58	14	24	21
Cd	215	77	43	98	136	63	201	57	128	108	157	139	bdl	78	76
Sn	249	124	105	82	80	73	bdl	80	143	164	170	64	85	bdl	108
Sb	298	181	162	121	116	268	180	122	166	55	301	115	130	149	196
Ba	893	593	221	130	515	574	683	435	1691	480	789	564	398	241	512
La	1123	917	636	734	908	1080	1511	582	1433	549	1041	814	754	443	687
Ce	2111	1124	820	987	797	1066	788	843	1469	599	1375	1051	845	891	738
Pr	2785	975	1965	1015	1651	725	915	923	1557	1167	1599	1528	950	547	864
Nd	3518	1997	2179	2137	2544	1470	2725	2069	3204	1771	2278	2203	1586	2727	2912
W	149	71	49	22	44	47	bdl	bdl	27	38	49	46	26	bdl	bdl
Pb	bdl	22	bdl	16	22	6	bdl	14	bdl	14	bdl	18	31	33	10
Bi	208	109	bdl	bdl	78	bdl	76	116	73	bdl	bdl	bdl	53	123	51

Continued….

analysis of procedural blanks, certified reference materials, duplicate samples, and analytical replicates to ensure analytical precision and accuracy. Analytical uncertainties for major and trace elements were generally maintained within acceptable international geochemical standards. Geochemical data reduction, statistical treatment, elemental variation diagrams, and petrogenetic discrimination plots were generated, using OriginPro 6.1 and Origin.

Results and Discussion

Field Observations

Regional geological context: Comprehensive field investigations within the Nyit Bruk Bisil sector of Shigar indicate pervasive pegmatitic intrusions emplaced within the metasedimentary and metavolcanic sequences of the Gilgit Formation. These pegmatites exhibit diverse morphologies including sheet-like, lensoidal, and discordant vein systems whose distribution is frequently governed by pre-existing fractures and shear zones. The observed structural patterns and vein geometries imply a polyphase magmatic emplacement history, with tectonic activity exerting a primary control on melt localization and vein propagation

Gilgit formation pegmatite (GP): The Gilgit Formation pegmatites form interconnected vein networks intruding metasedimentary, metavolcanic units, with emplacement structurally controlled by fractures and shear zones. Coarse biotite, muscovite ± feldspar assemblages indicate K-rich melts, whereas abundant tourmaline records localized boron (B) enrichment**.** Tourmaline and biotite enclosed within feldspar indicate progressive zoned crystallization, while local aquamarine (beryl) signifies Be enrichment, advanced fractional crystallization, and late-stage volatile concentration (Fig. 3).

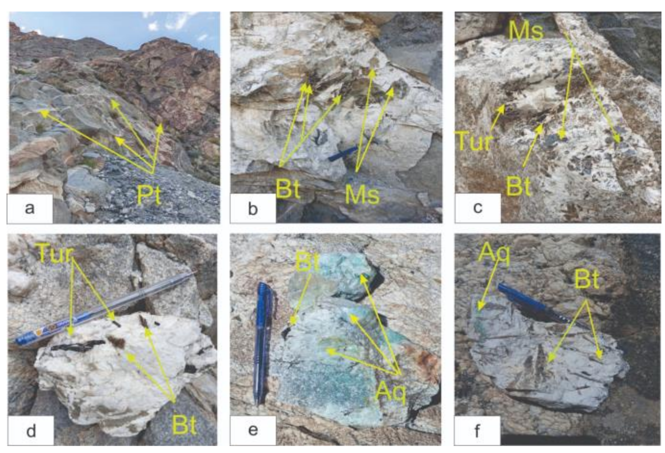

Fig. 3 Field photographs showing: (a) multiple pegmatite veins intruded into host rock, (b) biotite and muscovite mica minerals within a pegmatite vein, (c) pegmatite vein containing biotite, muscovite, and tourmaline crystals, (d) a hand specimen containing tourmaline and biotite embedded in feldspar, (e-f) the samples show biotite and bluish aquamarine crystals. **Abbreviations:** Pt = Pegmatite vein; Bt = Biotite; Ms = Muscovite Aq = Aquamarine; Tur = tourmaline.

Table 1 continued…

Sample	GP-46	GP-47	GP-48	GP-49	GP-50	GP-51	GP-52	GP-53	GP-54	GP-55	GP-56	GP-57	GP-58	GP-59	GP-60
SiO_2 (wt.%)	89.69	75.492	80.922	84.547	99.18	78.762	91.559	76.204	75.635	76.005	75.886	85.684	84.314	49.456	84.177
Al_2O_3	8.98	20.708	15.868	8.648	0.598	17.112	6.742	22.054	19.32	18.268	16.263	9.592	13.356	15.313	12.097
Fe_2O_3 (total)	0.288	0.237	0.572	5.149	0.058	1.188	0.421	0.037	0.525	3.333	3.227	0.332	0.575	22.486	0.683
MgO	bdl	bdl	bdl	bdl	bdl	bdl	bdl	bdl	bdl	bdl	1.294	1.648	bdl	8.445	bdl
CaO	0.598	2.953	2.188	0.63	0.041	2.57	1.088	1.532	4.111	1.932	3.113	2.536	1.406	3.033	2.848
TiO_2	0.393	0.59	0.401	0.885	0.107	0.309	bdl	0.14	0.344	0.348	0.156	0.18	0.302	1.005	0.108
MnO	0.051	0.019	0.048	0.141	0.016	0.06	0.19	0.033	0.065	0.114	0.06	0.029	0.047	0.222	0.087
P_2O_5	bdl	bdl	bdl	bdl	bdl	bdl	bdl	bdl	bdl	bdl	bdl	bdl	bdl	0.041	bdl
LE	664402	699147	704192	580502	538892	552161	555786	606505	580733	633513	621438	528551	570694	494252	609457
S	1725	1441	1890	1129	1366	1003	1546	1694	1084	1684	787	1356	1273	24449	1364
V	bdl	203	bdl	273	bdl	bdl	bdl	bdl	220	154	bdl	bdl	bdl	555	bdl
Cr	bdl	bdl	143	bdl	bdl	bdl	163	bdl	bdl	bdl	133	230	bdl	bdl	bdl
Co	104	64	54	bdl	58	124	bdl	60	bdl	bdl	119	74	bdl	bdl	60
Ni	bdl	bdl	86	bdl	38	bdl	30	17	26	19	62	50	bdl	38	bdl
Cu	34	22	1722	104	22	49	55	25	40	34	65	43	27	301	25
Zn	25	9	bdl	147	23	16	39	bdl	28	49	99	45	27	82	45
As	bdl	bdl	bdl	12	bdl	11	bdl	11	11	bdl	8	11	bdl	6	bdl
Se	20	7	9	8	14	3	5	10	9	14	7	12	8	14	6
Rb	65	40	45	223	13	52	575	57	229	157	49	84	159	15	61
Sr	321	134	300	200	19	278	22	1150	178	204	203	126	122	123	14
Y	15	9	20	16	14	35	15	14	31	8	7	23	12	48	29
Zr	31	28	52	38	28	34	112	bdl	92	56	32	92	107	72	72
Nb	34	28	32	38	22	24	14	29	34	34	20	36	24	21	61
Mo	41	36	54	40	39	30	29	46	49	47	23	47	45	81	24
Ag	27	23	19	27	37	39	40	30	47	32	54	33	21	42	46
Cd	201	170	263	148	136	148	189	48	144	84	96	146	141	168	55
Sn	154	127	169	79	48	103	53	115	bdl	95	78	63	61	bdl	60
Sb	bdl	123	216	116	97	98	146	218	91	279	124	bdl	149	191	136
Ba	2658	403	456	909	580	914	258	407	651	432	552	511	628	405	436
La	440	736	706	1285	717	1141	450	1059	816	599	1291	1031	1196	1161	899
Ce	995	809	564	977	1518	1093	865	588	1116	789	1083	981	1289	1022	1451
Pr	1549	1438	830	2220	2594	1195	1037	1105	1521	1533	2343	1586	1404	1938	1625
Nd	1816	1704	1516	3169	2779	1814	1594	1905	2531	2708	4895	1939	2299	2987	1526
W	bdl	29	26	73	24	36	27	33	40	bdl	32	36	24	144	34
Pb	10	27	7	29	bdl	31	60	17	39	20	13	6	38	bdl	32
Bi	67	59	125	66	48	bdl	103	39	48	87	98	109	82	36	bdl

Continued….

Nyit Bruk Bisil pegmatite (SP): The Nyit Bruk Bisil (SP) pegmatites are coarse-grained, leucocratic, quartz, and feldspar dominated bodies containing variable biotite, muscovite, tourmaline, spodumene, beryl, and locally aquamarine (Fig. 4).

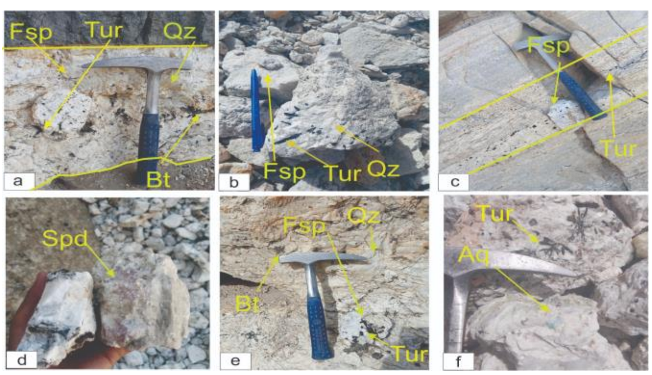

Fig. 4 Field photographs showing: **(a)** a pegmatite vein containing quartz, feldspar, biotite, muscovite, and tourmaline crystals, **(b)** a hand specimen containing tourmaline, quartz and feldspar, **(c)** a pegmatite vein containing feldspar and tourmaline crystals, **(d)** spodumene-bearing pegmatite **(e-f)** a pegmatite vein containing quartz feldspar biotite, Aquamarine and tourmaline crystals. **Abbreviations:** Pt = pegmatite vein; Bt = Biotite; Tur = Tourmaline; Aq = Aquamarine; Qz = Quartz; Fsp = Feldspar; Spd = spodumene.

Sharp contacts and vein orientations parallel to fractures and shear fabrics indicate structurally controlled emplacement. Marked mineralogical heterogeneity is expressed by tourmaline-rich, spodumene-bearing, and aquamarine-bearing domains within the felsic matrix. Coarse interlocking textures and localized late-stage feldspar, tourmaline overgrowths indicate crystallization from volatile-rich, highly evolved residual melts. The occurrence of spodumene, beryl, tourmaline, and aquamarine provides field evidence for rare-element enrichment and progressive magmatic fractionation, supporting the potential fertility of the SP pegmatites.

Discrimination between GP and SP Pegmatites

The Rb vs. Sr system reflects magmatic differentiation and melt fertility in granitic pegmatites. Rb, strongly incompatible, accumulates in residual melts, while Sr, compatible in plagioclase, is depleted during fractionation. Elevated Rb/Sr ratios thus indicate highly evolved melts with potential for LCT-type (Li, Cs, and Ta) pegmatites (London, 2018). In the Rb vs. Sr diagram (Fig. 5), GP pegmatites show moderate Rb, relatively high Sr, and low moderate Rb/Sr ratios, reflecting limited differentiation and early-stage melts with minimal rare-metal enrichment (Simmons *et al*., 2020). SP pegmatites display high Rb, strongly depleted Sr, and very high Rb/Sr ratios, indicating advanced feldspar fractionation, evolved residual melts, and fertile LCT-type pegmatites enriched in Li, Cs, Ta, Nb, Sn, and Be (London & Morgan, 2017).

Table 1 continued…

Sample	GP-61	GP-62	GP-63	GP-64	GP-65	GP-66	GP-67	GP-68	GP-69	GP-70	GP-71	GP-72	GP-73	GP-74	GP-75
SiO_2 (wt.%)	80.404	78.96	81.326	77.542	78.312	65.871	87.15	89.399	77.652	87.277	80.063	67.782	82.64	79.451	82.938
Al_2O_3	17.65	18.292	16.217	19.563	17.399	29.564	9.855	9.389	20.538	11.376	18.058	24.747	12.688	13.937	14.3
Fe_2O_3 (total)	0.219	0.369	0.285	0.285	1.519	3.142	0.905	0.431	0.131	0.087	0.137	0.145	0.263	1.859	0.348
MgO	bdl	bdl	bdl	bdl	bdl	bdl	bdl	bdl	bdl	bdl	bdl	2.038	2.861	2.763	bdl
CaO	1.456	2.278	1.99	2.044	2.169	0.913	2.042	0.429	1.477	0.873	1.478	4.928	1.259	1.465	2.046
TiO_2	0.231	bdl	0.121	0.514	0.543	0.428	bdl	0.195	0.152	0.325	0.233	0.331	0.25	0.448	0.349
MnO	0.039	0.101	0.061	0.051	0.057	0.082	0.047	0.157	0.049	0.062	0.031	0.029	0.039	0.077	0.02
P_2O_5	bdl	bdl	bdl	bdl	bdl	bdl	bdl	bdl	bdl	bdl	bdl	bdl	bdl	bdl	bdl
LE	592861	555183	572192	637757	660955	725305	587323	688916	590186	563059	525822	573898	594049	688493	593575
S	1319	1638	1299	1349	4773	1268	1325	1562	1787	1949	1728	2122	1711	1562	1588
V	bdl	bdl	bdl	bdl	bdl	bdl	131	bdl	187	bdl	203	bdl	bdl	bdl	bdl
Cr	bdl	bdl	bdl	bdl	bdl	94	bdl	bdl	bdl	92	289	267	bdl	bdl	bdl
Co	85	bdl	bdl	bdl	94	bdl	bdl	bdl	87	135	109	47	bdl	bdl	49
Ni	bdl	15	20	bdl	bdl	16	15	63	bdl	37	bdl	bdl	39	bdl	40
Cu	39	41	36	60	900	52	33	61	45	31	67	64	37	58	48
Zn	23	54	48	18	44	32	33	34	bdl	39	10	9	28	45	27
As	bdl	bdl	bdl	bdl	bdl	8	bdl	bdl	19	bdl	30	7	9	bdl	bdl
Se	12	7	8	9	bdl	9	10	10	7	11	14	6	2	13	10
Rb	347	151	57	68	336	87	29	666	243	197	273	15	141	64	46
Sr	240	198	137	129	157	100	320	40	236	442	672	671	338	503	749
Y	9	19	29	12	14	12	14	9	13	32	16	16	24	27	13
Zr	57	91	39	41	35	36	31	26	29	32	29	33	27	39	21
Nb	17	32	15	28	22	47	31	31	20	28	17	23	17	26	24
Mo	30	61	47	47	40	32	38	36	58	35	53	33	51	28	27
Ag	24	41	45	29	11	26	39	29	42	37	34	24	17	34	25
Cd	95	85	195	143	147	91	28	180	224	139	240	80	65	130	45
Sn	129	100	bdl	151	58	173	133	80	86	139	188	192	100	74	111
Sb	217	120	83	152	209	162	262	240	121	260	214	148	126	135	181
Ba	1113	996	668	391	335	425	764	534	959	2796	3174	504	2727	2505	1498
La	1210	987	980	546	469	839	999	525	1605	1062	562	343	701	814	421
Ce	1122	617	1192	445	847	536	1097	948	1515	407	422	813	791	1090	731
Pr	1399	1473	1100	1553	1026	1221	2116	1427	1814	838	1016	1768	596	1321	1466
Nd	2210	2094	2864	1965	1294	2462	3184	2035	1908	1168	1981	2669	1108	1727	2236
W	bdl	bdl	36	bdl	124	bdl	15	21	22	bdl	19	65	36	bdl	bdl
Pb	88	60	28	57	86	bdl	bdl	35	50	36	44	28	19	bdl	bdl
Bi	49	100	45	105	64	118	49	105	167	96	68	47	47	130	bdl

Continued…

Rb vs. Sr systematics track magmatic fractionation from weakly fertile GP to highly evolved, volatile-rich SP pegmatites, linking elevated Rb/Sr ratios to rare-metal enrichment and fertile LCT-type melts.

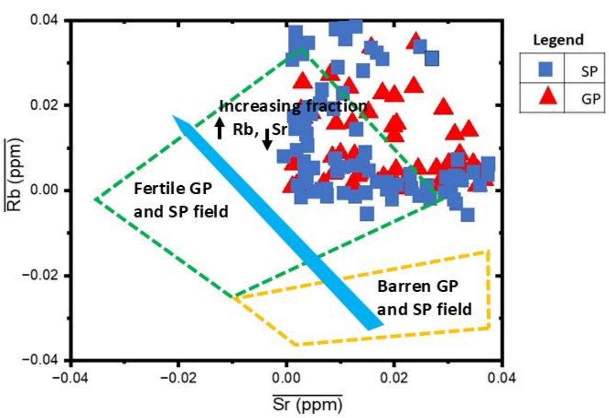

Fig. 5 Rb vs. Sr diagram of granitic pegmatites: fertile GP/SP show high Rb, low Sr; barren GP vs. SP show lower Rb higher Sr. Arrow indicates fractionation trend (after Cerny, 1991; London, 2008; Selway *et al*., 2005).

Pegmatite Affinity

Nb vs. Y systematics of the studied pegmatites indicate dominant LCT (Li, Cs, and Ta) affinity, reflecting HFSE-depleted, highly fractionated peraluminous granitic melts in an orogenic, syn-collisional setting; minor GP enrichment suggests localized LCT, NYF interaction, but low Nb/Y ratios exclude true NYF affinity (Wise *et al*., 2022). SP and GP pegmatites have likely derived from a common parental magma, with GP representing more evolved facies; Nb vs. Y systematics indicate LCT affinity with high Li, Ta, Cs, Rb potential, limited HFSE enrichment, and low Nb/Y ratios precluding significant NYF-type Nb vs. Y, REE mineralization (Wise & Brown, 2024; Fig. 6).

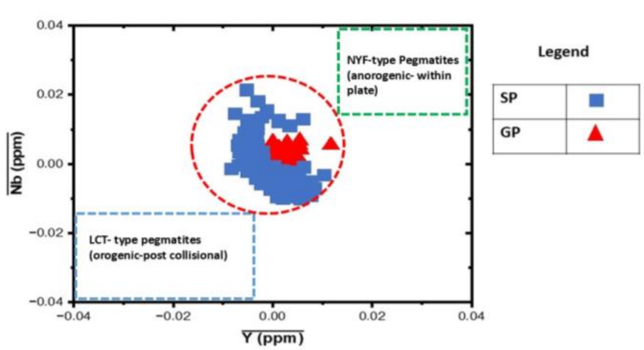

Fig. 6 Nb (ppm) vs. Y (ppm) pegmatite affinity diagram for SP and GP samples, showing schematic LCT (Li, Cs and Ta) and NYF (Nb, Y and F) domains. Fields are generalized after Cerny (1991) and Cerny and Ercit (2005).

Table 1 continued…

Sample	SP-1	SP-2	SP-3	SP-4	SP-5	SP-6	SP-7	SP-8	SP-9	SP-10	SP-11	SP-12	SP-13	SP-14	SP-15
SiO_2 (wt.%)	94.377	97.625	99.114	99.035	53.891	89.896	73.208	70.373	8.332	93.476	74.073	91.415	89.496	95.962	98.261
Al_2O_3	3.085	0.216	0.423	bdl	17.728	1.681	2.629	7.368	1.427	1.358	1.267	0.885	7.821	3.016	1.304
Fe_2O_3 (total)	1.303	0.657	0.108	0.569	14.037	0.78	1.226	4.884	0.241	1.542	9.107	1.335	1.024	0.243	0.271
MgO	bdl	bdl	bdl	bdl	bdl	bdl	2.412	bdl	36.11	2.724	bdl	3.605	bdl	bdl	bdl
CaO	0.79	1.131	0.229	0.124	13.238	7.206	19.885	16.056	53.671	0.715	14.588	2.432	0.933	0.173	0.146
TiO_2	0.386	0.32	0.107	0.221	0.69	0.326	0.47	0.609	0.178	0.107	0.269	0.217	0.681	0.571	bdl
MnO	0.058	0.052	0.019	0.051	0.335	0.111	0.171	0.471	0.041	0.079	0.697	0.044	0.046	0.036	0.017
P_2O_5	bdl	bdl	bdl	bdl	0.081	bdl	bdl	0.239	bdl	bdl	bdl	0.066	bdl	bdl	bdl
LE	589452	608891	562746	600665	645653	578634	647297	577117	647616	593838	613828	588401	574919	616681	631905
S	593	1489	1147	732	12787	1177	bdl	339	209	991	2884	911	3777	1047	727
V	151	335	bdl	151	bdl	222	bdl	444	bdl	bdl	bdl	bdl	bdl	bdl	bdl
Cr	207	bdl	bdl	623	bdl	118	100	bdl	bdl	bdl	172	272	bdl	bdl	bdl
Co	bdl	36	46	bdl	bdl	141	56	bdl	30	bdl	bdl	bdl	bdl	bdl	47
Ni	bdl	bdl	39	16	47	35	31	92	35	bdl	68	24	36	36	44
Cu	62	76	41	48	114	39	35	1143	58	64	33	73	42	39	37
Zn	27	29	37	10	57	59	43	131	33	14	34	82	34	46	36
As	97	17	9	17	bdl	bdl	bdl	27	9	bdl	9	bdl	bdl	8	bdl
Se	6	12	12	5	6	13	5	5	11	11	1	8	8	11	7
Rb	11	8	6	10	17	11	7	33	6	17	11	9	45	11	7
Sr	16	11	14	11	519	196	450	616	64	20	239	123	54	28	16
Y	13	7	19	15	84	44	69	59	29	11	23	20	12	16	18
Zr	31	15	26	15	1013	51	37	260	43	32	8	23	255	678	56
Nb	30	24	18	12	135	29	29	23	33	17	42	15	20	27	16
Mo	48	42	42	37	41	50	44	44	38	28	58	41	35	25	31
Ag	43	38	38	20	38	18	18	34	29	40	23	53	42	54	30
Cd	126	100	107	148	164	64	209	187	194	120	96	43	117	184	114
Sn	154	bdl	65	80	135	119	114	79	77	109	69	49	65	60	bdl
Sb	156	113	273	192	117	140	126	186	89	136	187	138	212	157	145
Ba	197	251	296	338	626	287	617	491	450	393	748	225	942	617	393
La	626	1175	1308	373	1459	844	776	930	988	865	872	584	1067	1447	817
Ce	327	1020	1158	644	1720	969	969	1255	1078	1274	946	1310	796	1185	728
Pr	679	1346	1307	917	1317	1120	971	1501	1242	1711	1585	710	1198	1679	1484
Nd	2395	2002	2938	1541	2118	2197	1444	1092	1587	3217	1843	3354	3076	3646	2431
W	bdl	58	21	45	32	bdl	bdl	80	bdl	50	bdl	34	bdl	bdl	15
Pb	bdl	bdl	bdl	bdl	30	15	bdl	43	bdl	bdl	bdl	113	bdl	bdl	9
Bi	48	36	79	34	124	98	126	106	127	44	bdl	bdl	42	104	66

Continued….

The Magmatic Differentiation Trend (SiO_2 vs. CaO)

The SiO_2 vs. CaO variation diagram (Fig. 7) displays a well-defined negative correlation for both SP and GP samples, reflecting progressive magmatic differentiation during fractional crystallization. The systematic decrease in CaO with increasing SiO_2 indicates the early removal of Ca-bearing mineral phases, primarily clinopyroxene and calcic plagioclase, from the evolving magma. Such trends are widely recognized as characteristic of calc-alkaline magmatic systems, where crystallization of mafic silicates and plagioclase progressively depletes CaO while enriching the residual melt in silica (Wilson, 1989). The distribution of the samples broadly follows an evolutionary trajectory from basaltic to intermediate and felsic compositions, consistent with differentiation pathways observed in many arc-related magmatic suites (White, 2013).

Similar SiO_2 vs. CaO fractionation trends have been documented in experimental and natural systems, and are interpreted as evidence for progressive crystal, liquid separation during magma ascent and storage within crustal reservoirs (Grove *et al*., 2012). Orderly, the overlap of SP and GP samples along the same differentiation array suggests that both groups likely originated from a genetically related parental magma, but experienced variable degrees of fractional crystallization and magma evolution. The more evolved compositions characterized by higher SiO_2 and lower CaO reflect advanced differentiation stages, possibly associated with prolonged magma residence and crystal fractionation within upper crustal magma chambers.

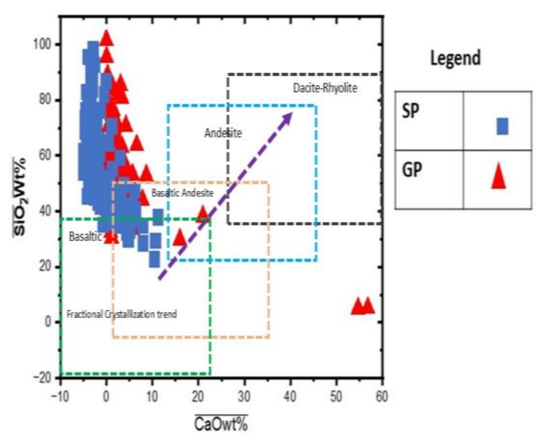

Fig. 7 SiO_2 vs. CaO variation diagram for SP and GP samples showing a negative correlation indicative of fractional crystallization controlled by Ca-rich mineral removal along a typical calc-alkaline magmatic differentiation trend (Bowen, 1928; Wilson, 1989; White, 2013).

In contrast, a small number of samples plotting at extremely high CaO values deviate from the main magmatic trend and may represent carbonate-rich lithologies, calcite-bearing alteration assemblages, or secondary processes such as

Table 1 continued

Sample	SP-16	SP-17	SP-18	SP-19	SP-20	SP-21	SP-22	SP-23	SP-24	SP-25	SP-26	SP-27	SP-28	SP-29	SP-30
SiO_2 (wt.%)	23.086	98.557	99.146	95.675	40.773	93.511	78.865	79.942	86.129	84.588	79.962	84.634	84.78	97.636	80.895
Al_2O_3	2.382	0.492	0.307	bdl	6.268	3.996	19.19	18.057	11.819	12.922	15.7	12.945	13.009	0.233	15.976
Fe_2O_3 (total)	2.348	0.296	0.108	0.215	5.596	0.208	0.982	1.166	0.837	0.195	0.488	1.304	0.245	0.061	0.167
MgO	2.561	bdl	bdl	3.666	14.693	1.673	bdl	bdl	bdl	1.557	3.092	bdl	bdl	2.023	bdl
CaO	68.314	0.397	0.223	0.212	31.596	0.358	0.475	0.466	0.589	0.38	0.462	0.468	1.651	0.021	2.466
TiO_2	1.214	0.222	0.19	0.181	0.891	0.216	0.131	0.178	0.168	0.161	0.17	0.433	0.279	0	0.471
MnO	0.095	0.036	0.026	0.052	0.183	0.038	0.194	0.061	0.238	0.042	0.073	0.061	0.036	0.027	0.025
P_2O_5	bdl	bdl	bdl	bdl	bdl	bdl	0.163	0.13	0.22	0.156	0.053	0.154	bdl	bdl	bdl
LE	562828	604886	602586	662392	628622	587987	635719	604731	620489	583154	600683	609342	599341	610624	656298
S	bdl	823	997	1071	bdl	1232	1047	510	3940	748	973	1217	884	492	781
V	bdl	bdl	bdl	bdl	229	bdl	188	bdl	bdl	bdl	365	bdl	bdl	91	bdl
Cr	120	bdl	bdl	bdl	bdl	bdl	bdl	bdl	bdl	bdl	bdl	bdl	bdl	261	bdl
Co	bdl	97	103	bdl	200	bdl	bdl	bdl	bdl	50	112	123	68	45	61
Ni	22	bdl	bdl	bdl	96	22	78	bdl	64	33	28	36	69	25	bdl
Cu	71	56	38	72	65	13	48	27	28	44	46	66	48	43	15
Zn	25	29	31	20	80	12	52	86	85	54	28	62	26	30	9
As	31	5	bdl	11	bdl	16	bdl	bdl	bdl	21	bdl	bdl	9	3	17
Se	bdl	4	10	bdl	15	8	8	8	5	11	4	10	5	6	bdl
Rb	10	7	14	12	26	18	338	418	326	205	164	447	287	7	34
Sr	304	18	13	8	189	21	19	14	20	36	23	27	85	12	112
Y	24	12	13	10	47	19	22	16	34	23	17	21	9	15	29
Zr	79	22	23	26	320	142	26	30	21	38	21	21	28	26	61
Nb	36	23	18	25	25	13	38	34	19	23	21	22	17	32	23
Mo	74	24	30	35	23	37	45	42	22	50	24	34	25	31	24
Ag	36	22	38	17	54	18	11	21	43	37	27	31	29	24	16
Cd	214	92	129	bdl	230	135	102	78	123	122	159	71	146	116	77
Sn	0	64	97	73	160	79	179	55	83	129	bdl	146	46	151	108
Sb	302	80	155	187	90	127	244	182	bdl	236	98	225	146	187	255
Ba	502	331	496	177	426	871	403	376	250	394	351	294	611	360	409
La	1618	778	1414	545	708	964	706	537	306	654	868	686	561	687	860
Ce	1413	784	692	762	810	1007	973	985	734	1116	522	848	770	1069	535
Pr	1232	1254	1049	1229	1583	1870	1562	2566	972	1771	1411	668	847	1685	868
Nd	2930	1898	1191	1519	2370	2277	2243	1857	1284	1906	2352	1448	2175	2254	1394
W	bdl	58	bdl	bdl	51	52	28	bdl	32	70	54	54	17	bdl	38
Pb	bdl	bdl	bdl	bdl	bdl	bdl	26	26	52	24	30	bdl	76	bdl	42
Bi	bdl	bdl	41	79	126	30	64	96	62	bdl	61	85	bdl	53	bdl

Continued….

crustal contamination and hydrothermal modification rather than primary magmatic compositions. Mainly, the coherent differentiation pattern defined by the majority of samples supports a petrogenetic model dominated by fractional crystallization of Ca-rich phases, consistent with the evolutionary behavior of calc-alkaline magmatic systems in subduction-related tectonic environments (Jagoutz & Kelemen, 2015).

Li vs. Rb Fertility

Most pegmatites plot in the moderately evolved field, with some reaching the Li, Cs, and Ta (LCT) field, reflecting magmatic differentiation and fractional crystallization that concentrate Li and Rb; barren granites remain low in these elements (London, 2008; Fig.8). Li vs. Rb trends track melt evolution and pegmatite fertility: LCT pegmatites derive from extreme fractionation of peraluminous granitic melts, enriching incompatible elements, while less evolved pegmatites are poor in Li and Rb (London, 2008).

Li-rich pegmatites show lower Zr/Hf, K/Rb, Rb/Ba, and higher SiO_2 than coexisting granites, consistent with late stage melt enrichment (Ye *et al*., 2024). Li isotopes indicate magmatic differentiation and fluid, melt interactions, while partial melting or remelting of fractionated granites can also produce Li-rich melts (Koopmans *et al*., 2024). High Li and Rb reliably indicate fertile melts forming spodumene and lepidolite-bearing LCT pegmatites, whereas low values denote barren systems, providing a robust exploration framework (Koopmans *et al*., 2024).

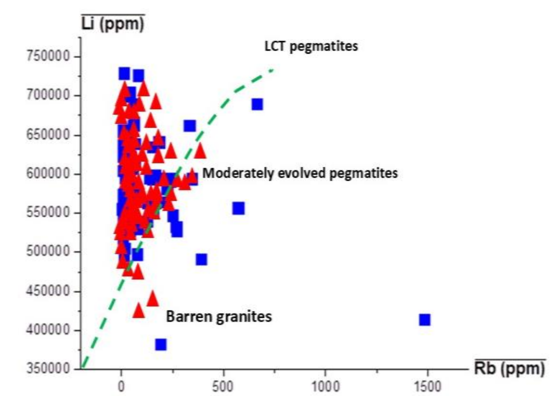

Fig. 8 Li vs. Rb (ppm) in granites and pegmatites. Most pegmatites are moderately evolved; a few reach LCT fields, while barren granites remain low, reflecting magmatic differentiation and fractionation (London, 2008).

Geochemical Data

The Li vs. Rb systematics provide important information on the degree of magmatic fractionation and elemental enrichment within the studied pegmatites. In addition, Ta, Be discrimination is employed to further evaluate pegmatite type and their geochemical evolution.

Li vs. Rb Systematics

The Li vs. Rb variation diagram (Fig. 9) highlights distinct

Table 1 continued…

Sample	SP-31	SP-32	SP-33	SP-34	SP-35	SP-36	SP-37	SP-38	SP-39	SP-40	SP-41	SP-42	SP-43	SP-44	SP-45
SiO_2 (wt.%)	86.644	82.494	82.745	76.957	96.021	82.21	80.136	87.603	84.087	80.416	74.211	87.018	95.545	75.999	77.792
Al_2O_3	12.466	14.072	14.273	14.551	2.713	15.536	18.197	10.697	13.897	16.31	17.585	11.824	3.738	20.926	17.296
Fe_2O_3 (total)	0.149	0.388	0.835	0.855	0.327	0.603	0.286	0.292	0.756	0.751	2.729	0.151	0.196	1.234	1.253
MgO	bdl	bdl	bdl	4.239	bdl	bdl	bdl	bdl	bdl	bdl	3.759	bdl	bdl	bdl	2.538
CaO	0.626	2.369	1.95	2.842	0.473	0.979	1.247	0.862	0.975	2.173	1.17	0.748	0.11	1.462	0.468
TiO_2	bdl	0.567	0.157	0.502	0.427	0.621	0.103	0.374	0.239	0.296	0.448	0.214	0.389	0.202	0.431
MnO	0.056	0.056	0.04	0.053	0.038	0.051	0.03	0.078	0.046	0.053	0.046	0.045	0.021	0.056	0.177
P_2O_5	0.059	0.053	bdl	bdl	bdl	bdl	bdl	0.095	bdl	bdl	0.051	bdl	bdl	0.122	0.045
LE	583949	666060	645707	595317	674611	658956	570791	656808	618982	568594	582901	659893	540693	599194	631577
S	5153	1033	682	1015	1810	938	1104	994	1288	944	536	866	843	1122	703
V	199	bdl	bdl	130	bdl	178	bdl	213	bdl	bdl	bdl	bdl	bdl	bdl	158
Cr	bdl	bdl	122	bdl	bdl	bdl	bdl	bdl	bdl	bdl	224	bdl	141	bdl	bdl
Co	23	45	178	48	bdl	111	bdl	116	bdl	108	bdl	97	67	bdl	151
Ni	bdl	bdl	37	26	bdl	bdl	39	104	35	bdl	36	bdl	50	33	61
Cu	25	33	47	63	70	49	100	97	34	19	43	37	29	60	25
Zn	31	19	22	46	33	18	27	75	30	51	37	34	21	49	25
As	27	bdl	bdl	34	5	15	32	13	19	bdl	24	bdl	bdl	bdl	10
Se	6	9	10	7	5	14	6	5	14	11	16	12	2	5	9
Rb	656	112	191	236	5	222	388	191	465	284	397	247	46	180	434
Sr	29	102	82	105	5	67	89	65	123	140	116	55	7	43	17
Y	36	33	104	38	13	10	31	451	26	12	53	36	16	25	20
Zr	16	31	94	53	33	26	41	50	24	30	66	47	27	33	20
Nb	19	17	29	23	26	25	21	10	34	36	30	30	24	45	126
Mo	29	31	24	35	35	38	41	44	41	33	32	39	48	25	27
Ag	28	26	31	32	32	26	48	15	50	42	32	24	55	44	46
Cd	164	90	138	181	80	39	177	92	181	34	157	92	163	59	141
Sn	170	103	141	89	51	242	39	77	144	103	45	212	85	123	46
Sb	168	103	139	108	126	335	133	90	236	176	98	236	231	176	148
Ba	208	412	504	342	541	454	456	720	1087	906	477	377	388	563	275
La	915	448	594	587	1204	524	658	797	926	628	817	1054	603	819	1110
Ce	1084	576	660	410	1106	780	589	755	888	1415	622	1067	1129	760	669
Pr	1377	1150	1031	1113	2035	1925	1555	1187	1508	1901	896	840	970	1354	839
Nd	3473	1575	2407	3221	2985	1659	2430	2361	1327	2959	2842	1584	2694	2319	2005
W	36	bdl	bdl	34	bdl	81	26	bdl	66	bdl	58	22	bdl	109	38
Pb	14	78	29	43	bdl	46	66	33	88	85	83	35	bdl	35	bdl
Bi	135	bdl	40	bdl	90	161	40	75	58	42	bdl	149	77	67	52

Continued….

geochemical trends between the SP and GP sample groups, and provides insight into the degree of magmatic differentiation within the studied granitoid and pegmatite system. Lithium (Li) and rubidium (Rb) are incompatible elements that preferentially partition into residual melts during fractional crystallization of granitic magmas. Consequently, their progressive enrichment is widely used as a geochemical indicator of advanced magmatic evolution and pegmatite formation (Muller *et al*., 2022). The SP samples show a broad range of Rb concentrations, from background levels (<500 ppm) to extremely enriched values (>3000 ppm), while Li contents remain relatively moderate (~30–40 ppm).

The majority of SP samples plot within the background rock field, suggesting derivation from relatively primitive granitoids or weakly fractionated melts. However, several SP samples fall within the fractionated granite field (500–2500 ppm Rb), reflecting progressive fractional crystallization processes involving feldspar and mica, which preferentially incorporate incompatible elements into the residual melt. Notably, one SP sample plots within the pegmatite field with Rb concentrations approaching ~3500 ppm. Such extreme enrichment is characteristic of highly evolved granitic systems that can generate rare-metal pegmatites. Recent studies indicate that lithium-rich pegmatites commonly originate from highly fractionated melts derived either from evolved granitic magmas or from partial melting of Li-enriched metasedimentary sources, followed by further enrichment through fractional crystallization and fluid-assisted processes (Koopmans *et al*., 2024; Yuan *et al*., 2023; Chen *et al*., 2024).

Elevated Rb concentrations are particularly diagnostic of LCT-type pegmatites (Li, Cs, and Ta), where incompatible elements become concentrated in late-stage melts and magmatic fluids (Yuan *et al*., 2023). In contrast, the GP samples cluster mainly within the background to weakly fractionated granite field, characterized by relatively low Rb (<500 ppm) and Li values generally below ~25 ppm. This distribution suggests that the GP suite represents relatively primitive or moderately evolved granitic compositions that have not undergone extensive magmatic differentiation. The gradual increase of Rb with Li within this group likely reflects limited fractional crystallization without reaching the advanced stages required for pegmatite generation.

Overall, the diagram indicates two distinct evolutionary trends within the studied system. The SP samples reflected a more evolved magmatic trajectory, with evidence for strong incompatible element enrichment and possible transition toward pegmatitic compositions. In contrast, the GP samples represent less evolved granitoid compositions with limited geochemical fractionation. Such patterns are consistent with recent models of granite and pegmatite systems in which rare-element pegmatites form during the late stages of magmatic evolution through a combination of fractional crystallization, partial melting of enriched crustal sources, and magmatic-

Table 1 continued…

Sample	SP-46	SP-47	SP-48	SP-49	SP-50	SP-51	SP-52	SP-53	SP-54	SP-55	SP-56	SP-57	SP-58	SP-59	SP-60
SiO_2 (wt.%)	80.061	76.63	81.469	78.826	80.344	58.037	84.509	74.8	82.3	80.851	76.354	82.731	85.258	79.242	94.65
Al_2O_3	17.322	20.143	16.487	18.518	17.065	17.832	10.559	20.828	14.561	16.059	20.498	15.341	12.859	17.156	4.327
Fe_2O_3 (total)	1.534	0.893	0.617	1.07	1.403	17.475	3.676	0.501	2.237	1.084	0.613	0.842	1.343	0.573	0.633
MgO	bdl	bdl	bdl	bdl	bdl	2.951	bdl	1.784	bdl	bdl	bdl	bdl	bdl	bdl	bdl
CaO	0.7	1.828	0.694	1.262	0.908	0.906	0.514	2.036	0.691	1.302	2.26	0.655	0.194	2.478	0.178
TiO_2	0.18	0.3	0.291	0.277	0.251	2.258	0.54	bdl	0.151	0.65	0.237	0.289	0.241	0.466	0.185
MnO	0.099	0.036	0.094	0.046	0.029	0.428	0.069	0.051	0.059	0.055	0.038	0.042	0.022	0.085	0.028
P_2O_5	0.104	0.169	0.349	bdl	bdl	0.113	0.134	bdl	bdl	bdl	bdl	0.1	0.083	bdl	bdl
LE	569998	597277	607826	610689	646082	673162	591331	603395	604761	622670	642981	604408	629198	668504	634739
S	752	2060	702	1326	1094	657	1182	958	993	842	715	924	1478	790	3165
V	276	bdl	217	bdl	bdl	bdl	bdl	bdl	188	122	131	bdl	bdl	bdl	bdl
Cr	bdl	206	bdl	bdl	bdl	207	bdl	76	bdl	bdl	bdl	bdl	bdl	328	bdl
Co	115	bdl	66	141	bdl	bdl	bdl	45	297	bdl	50	88	74	bdl	39
Ni	34	bdl	21	20	bdl	27	25	54	18	bdl	bdl	42	39	bdl	55
Cu	67	43	20	73	22	52	21	53	51	59	40	48	18	73	46
Zn	117	34	36	25	27	309	58	19	69	44	33	45	33	19	23
As	120	bdl	14	bdl	bdl	bdl	bdl	bdl	14	14	bdl	bdl	bdl	bdl	bdl
Se	6	5	8	8	15	7	9	10	4	15	8	20	11	6	11
Rb	999	3038	373	514	703	602	471	180	414	192	174	558	81	51	149
Sr	16	61	13	93	63	104	117	37	34	103	32	28	13	369	42
Y	29	bdl	28	31	44	28	7	20	26	89	73	33	39	6	8
Zr	12	21	17	33	25	9	30	37	31	10	27	37	40	22	46
Nb	33	39	60	22	15	69	26	35	58	13	23	40	28	21	28
Mo	22	53	38	37	39	39	33	42	40	21	44	16	28	25	29
Ag	45	26	27	35	27	31	10	24	45	17	46	16	26	38	30
Cd	165	164	51	72	34	99	101	100	61	192	138	190	96	132	154
Sn	109	84	192	169	139	329	101	136	164	157	186	87	128	86	120
Sb	155	131	263	182	198	424	201	159	248	217	321	107	155	219	117
Ba	610	220	341	512	332	1234	1806	417	480	634	418	309	327	457	507
La	1021	1059	702	642	579	931	1060	406	750	961	1084	909	529	675	888
Ce	1293	1018	974	487	852	937	321	843	653	733	1132	577	1347	865	770
Pr	1550	1535	1199	1441	1204	2075	1029	1561	1263	1886	1850	1187	876	1171	1239
Nd	2749	2272	886	1817	3136	1975	1903	1762	2027	1633	2437	1699	1123	1255	1576
W	bdl	21	bdl	33	29	48	29	58	80	bdl	33	bdl	bdl	32	bdl
Pb	13	17	bdl	95	113	39	67	52	15	33	28	51	bdl	87	8
Bi	bdl	89	bdl	bdl	102	88	35	65	bdl	bdl	41	107	101	50	69

Continued….

hydrothermal processes (Chen *et al*., 2024).

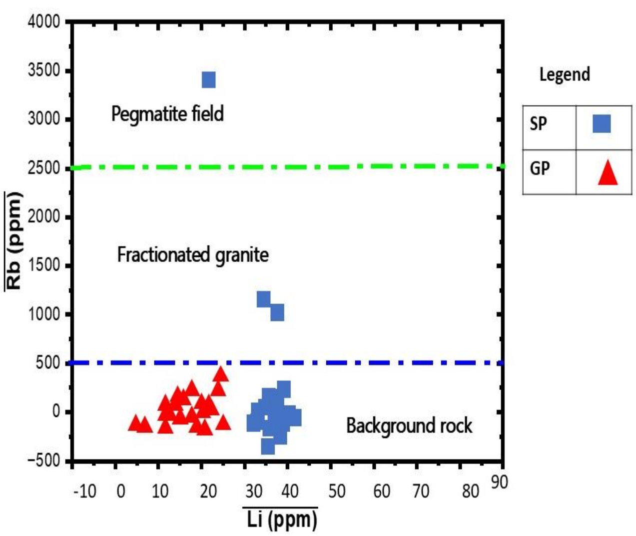

Fig. 9 Li vs. Rb variation diagram showing SP and GP samples. Dashed lines separate background rocks (<500 ppm Rb), fractionated granites (500–2500 ppm), and pegmatite fields (>2500 ppm). SP samples indicate stronger magmatic differentiation, whereas GP samples reflect weakly evolved granitoids (Koopmans et al., 2023; Yuan et al., 2023).

Ta vs. Be Discrimination in Pegmatites

The Ta vs. Be bivariate diagram (Fig.10) provides a robust geochemical discriminator for pegmatite subtypes, effectively separating spodumene-type pegmatites (SP) from gneissic or garnet, mica pegmatites (GP). Beryllium behaves as a strongly incompatible lithophile element during pegmatitic melt evolution and is preferentially hosted in beryl, whereas tantalum, a high-field-strength element (HFSE), becomes progressively enriched in highly fractionated rare-element pegmatites and is typically accommodated by columbite-group minerals (CGM) and microlite.

Consequently, the absolute abundances and covariation of Ta and Be serve as sensitive proxies for melt differentiation and rare-metal fertility (Selway *et al*., 2022). The SP samples define a positive Ta vs. Be covariation trend, with Ta concentrations typically ranging from ~20 to >100 ppm and be from ~20 to 100 ppm, consistent with advanced magmatic fractionation (Fig. 10). In spodumene-bearing systems, peraluminous Li-rich melts enriched in fluxing components (F, B, P) significantly enhance the complexing capacity and solubility of HFSEs such as Ta and Nb (Linnen *et al*., 2023). Elevated Ta concentrations within this field suggest crystallization from highly evolved residual melts approaching the cleavelandite, lepidolite stages of pegmatite evolution, during which progressive fractionation increases

Table 1 continued…

Sample	SP-61	SP-62	SP-63	SP-64	SP-65	SP-66	SP-67	SP-68	SP-69	SP-70	SP-71	SP-72	SP-73	SP-74	SP-75
SiO_2 (wt.%)	74.53	58.162	74.424	77.088	78.578	72.801	71.82	80.825	86.198	82.034	83.211	79.225	71.56	72.772	78.692
Al_2O_3	23.185	34.957	24.4	21.008	17.641	19.114	21.206	17.437	10.563	12.62	14.941	18.984	25.435	24.743	18.775
Fe_2O_3 (total)	0.799	5.354	0.111	0.157	0.376	5.374	4.658	0.909	1.777	1.737	0.468	0.655	0.353	0.364	1.934
MgO	bdl	bdl	bdl	bdl	2.263	bdl	bdl	bdl	bdl	1.929	bdl	bdl	bdl	bdl	bdl
CaO	0.835	0.78	0.417	1.047	0.914	0.657	0.933	0.38	1.029	1.116	0.871	0.915	2.355	1.79	0.522
TiO_2	0.325	0.564	0.321	0.292	0.191	0.306	0.487	0.286	0.395	0.462	0.295	0.194	0.233	0.289	0
MnO	0.063	0.184	0.21	0.048	0.037	1.749	0.756	0.108	0.039	0.102	0.09	0.027	0.065	0.041	0.077
P_2O_5	0.263	bdl	0.118	0.36	bdl	bdl	0.14	0.055	bdl	bdl	0.124	bdl	bdl	bdl	bdl
LE	592336	601782	585019	644800	609541	632924	564594	575938	656437	654570	645195	555148	654672	664053	563908
S	878	1014	775	1054	1075	1154	711	958	722	727	1137	1671	853	708	884
V	bdl	bdl	bdl	bdl	bdl	bdl	bdl	bdl	bdl	212	bdl	bdl	473	bdl	bdl
Cr	303	bdl	bdl	bdl	108	bdl	bdl	105	bdl	70	bdl	184	bdl	bdl	85
Co	bdl	273	59	74	46	bdl	bdl	bdl	bdl	77	100	bdl	bdl	102	267
Ni	88	52	bdl	49	bdl	44	31	48	bdl	26	40	bdl	46	28	33
Cu	44	70	54	32	88	200	71	63	43	46	51	27	159	54	36
Zn	50	379	46	30	20	108	173	36	40	49	43	15	24	39	126
As	25	bdl	39	32	bdl	bdl	bdl	bdl	bdl	bdl	bdl	bdl	26	bdl	13
Se	12	10	16	10	10	10	5	10	10	7	9	11	8	5	11
Rb	524	1703	8644	2141	1007	415	682	990	35	41	181	466	35	57	857
Sr	37	20	31	22	17	14	18	15	221	154	57	103	737	512	22
Y	16	bdl	48	bdl	33	36	35	32	25	33	26	16	8	15	11
Zr	26	29	bdl	18	20	109	84	29	32	62	24	54	33	126	28
Nb	22	239	136	24	28	972	93	151	38	27	46	52	21	28	43
Mo	21	35	60	51	50	47	47	30	45	40	37	48	33	41	53
Ag	29	40	35	10	51	29	16	28	35	23	43	19	24	20	11
Cd	105	145	231	72	135	89	156	87	36	93	86	76	65	33	115
Sn	105	747	479	87	109	99	70	163	72	119	99	72	132	bdl	136
Sb	184	463	268	106	78	148	199	358	189	51	214	229	119	231	74
Ba	567	336	294	135	135	379	387	496	543	382	314	449	250	286	623
La	443	741	748	320	555	793	634	477	874	726	816	711	921	530	1226
Ce	530	637	1299	425	780	1153	1049	696	1109	866	515	1116	923	647	732
Pr	770	953	2418	1497	1908	1762	2202	1646	1115	774	736	1220	1175	703	1737
Nd	1172	1689	3331	2774	2436	2271	1171	2506	2118	2266	1523	1972	1796	1565	1855
W	bdl	116	254	18	53	215	85	166	bdl	bdl	bdl	55	26	29	29
Pb	75	bdl	bdl	bdl	75	34	23	17	13	16	7	427	30	38	bdl
Bi	85	101	124	125	62	52	bdl	39	44	175	84	37	42	107	101

Note: LE = lower error limit; bdl = below detection limit. Major element concentrations are reported in wt. %, whereas trace and REE concentrations are given in ppm. Cl, Hg, and Th were analyzed but remained below the respective detection limits in all GP and SP samples and are therefore omitted from the table.

Ta/Nb ratios and promotes the stabilization of Ta-dominant CGM phases (Cerny*et al*., 2021). In contrast, the GP samples cluster at relatively low Ta concentrations (<20 ppm) and moderate Be contents, indicating weakly fractionated pegmatitic melts that are typically barren or only weakly mineralized with respect to rare metals (Fig. 10). These pegmatites most likely represent melts generated by local anatexis of metasedimentary protoliths, where limited fractional crystallization prevented the attainment of Ta saturation or the development of economically significant rare-metal mineralization (Muller *et al*., 2024).

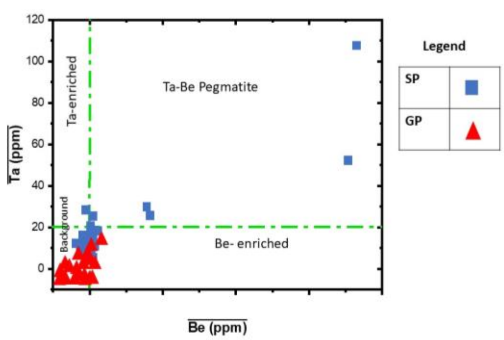

Petrogenetic and Exploration Implications

The compositional separation between SP and GP fields indicates that Ta and Be fractionation pathways diverge during early pegmatite evolution but converge in highly evolved melts (Fig. 10). The SP trend is consistent with boundary-layer enrichment and dis-equilibrium crystallization models, in which Ta becomes concentrated in late-stage residual melt films along crystal, melt interfaces during progressive undercooling (Thomas & Davidson, 2012). The lack of intermediate compositions suggests a petrogenetic discontinuity: GP pegmatites likely represent locally derived anatectic melts that crystallized in situ, whereas SP pegmatites represent migrated, highly fractionated melts within a more evolved magmatic plumbing system (Vieira *et al*., 2023).

From an economic geology perspective, elevated Ta and Be concentrations, particularly within the high-Ta segment of the SP field, provide a reliable vector toward Li, Cs, and Ta (LCT) pegmatite mineralization (Fig. 2). Samples occupying this compositional domain constitute priority targets for further evaluation of Ta and potentially Li resources (Kesler *et al*., 2022). Importantly, the diagram illustrates that bulk-rock Be concentrations alone are insufficient indicators of pegmatite fertility; rather, the systematic covariation of Ta and Be provides a more reliable geochemical criterion for identifying highly evolved, mineralization-prone pegmatitic systems.

Petrogenesis

The geochemical and structural characteristics of KLIA pegmatites indicate that progressive magmatic differentiation

Table 2. Whole-rock trace element concentrations (ppm) for the GP and SP sample suites.

Sample Name	Li	Rb	Be	Ta	Cs	La	Sr	Au	Y	Nd	Pb	Zn	Ba	Mg
	ppm or %age	ppm or %age	ppm or %age	ppm or %age	ppm or %age	ppm or %age	ppm or %age	ppm or %age	ppm or %age	ppm or %age	ppm or %age	ppm or %age	ppm or %age	ppm or %age
GP-1	<10.00	10	--	--	--	--	--	--	--	--	--	--	--	0.76
GP-2	<10.00	<1.00	<5.00	--	--	--	--	--	--	--	--	--	--	--
GP-3	<10.00	--	--	--	--	--	--	--	--	--	--	--	--	--
GP-4	<10.00	16	--	--	--	--	--	--	--	--	--	--	--	--
GP-5	<10.00	<1.00	<5.00	--	--	--	--	--	--	--	--	--	--	--
GP-6	<10.00	<1.00	--	--	--	--	--	--	--	--	--	--	--	--
GP-7	13	150	--	15	114	--	--	--	--	--	--	--	--	--
GP-8	13	139	--	5	108	--	--	--	--	--	--	--	--	--
GP-9	<10.00	99	--	--	--	--	--	--	--	--	--	--	285	--
GP-10	<10.00	23	<5.00	--	--	--	--	--	--	--	--	--	--	--
GP-11	14	118	<5.00	--	--	--	--	--	--	--	--	--	--	--
GP-12	<10.00	94	--	--	--	--	--	--	--	--	--	--	--	--
GP-13	<10.00	62	<5.00	--	--	--	--	--	--	--	--	--	--	--
GP-14	18	321	--	27	94	--	--	--	--	--	--	--	--	--
GP-15	<10.00	69	<5.00	--	--	--	--	--	--	--	--	--	--	--
GP-16	16	<1.00	<5.00	--	--	--	--	--	--	--	--	--	--	--
GP-17	<10.00		--	--	--	--	--	--	--	--	--	--	--	--
GP-18	<10.00	<1.00	--	--	--	--	--	--	--	--	--	--	--	--
GP-19	<10.00	1	--	--	--	--	--	--	--	--	--	--	--	--
GP-20	Nd	--	--	--	--	--	--	<0.02	--	--	--	--	--	--
SP-1	<10.00	<1.00	<5.00	<5	--	--	--	--	--	--	--	--	--	--
SP-2	<10.00	<1.00	--	--	--	--	--	--	--	--	--	--	--	--
SP-3	<10.00	<1.00	<5.00	--	--	--	--	--	--	--	--	--	--	--
SP-4	<10.00	<1.00	<5.00	--	--	--	--	--	--	--	--	--	--	--
SP-5	10	<1.00	<5.00	--	--	--	--	--	--	--	--	--	--	--
SP-6	50	138	8	<5	<1.00	--	9	--	--	--	--	--	--	--
SP-7	40	<1.00	12	--	--	--	--	--	--	--	--	--	--	--
SP-8	30	36	9	--	<1	--	58	--	--	--	--	--	--	--
SP-9	30	163	5	--	<1.00	--	--	--	--	--	--	--	--	--
SP-10	20	12	11	<5	--	--	25	--	--	--	--	--	--	--
SP-11	60	155	5	<5	--	--	67	--	--	--	--	--	--	--
SP-12	40	377	5	--	--	--	41	--	--	--	--	--	--	--
SP-13	60	--	--	--	<1.00	--	--	--	--	--	--	--	--	--
SP-14	40	--	--	--	53	--	--	--	--	--	--	--	--	--
SP-15	10	193	13	--	--	--	--	--	--	--	--	--	--	--
SP-16	5900	3480	38	50	<1.00	--	2	--	--	--	--	--	--	--
SP-17	10	522	47	104	--	--	4	--	--	--	--	--	--	--
SP-18	20	<1.00	--	--	--	--	--	--	--	--	--	--	--	--
SP-19	60	355		11	<5	4	--	14	--		--	--	--	--

and structural focusing of volatile-rich residual melts werethe principal controls on rare-metal enrichment. Fertile pegmatites are enriched in Li, Rb, Cs, Nb, Ta, Sn and exhibit high Rb/Sr and Cs/Rb but low K/Rb, consistent with highly fractionated peraluminous granitic melts (Cerny *et al*., 2012; Linnen *et al*., 2012). Progressive crystallization concentrated H_2O, B, F, and P in residual melts, enhancing HFSE mobility and promoting Li, Ta mineral saturation (Muller *et al*., 2022). Shear zones, fractures, and lithological contacts subsequently focused these evolved melts into favorable crustal sites, consistent with structurally controlled orogenic LCT pegmatite emplacement (Koopmans *et al*., 2024). Positive Ta, Be and Li, Rb relationships and systematic Rb/Sr, Cs/Rb, and K/Rb variations further distinguish fertile from less evolved barren pegmatites (Yuan *et al*., 2023). Thus, KLIA pegmatite fertility reflects coupled source enrichment, fluid-assisted melting, extreme fractionation, and structural focusing**,** providing an effective exploration framework based on Li, Rb, Cs, and Ta systematics and structural architecture.

The conceptual model (Fig. 11) depicts a subduction, arc, and crustal melting system in which slab dehydration metasomatizes the mantle wedge and supplies incompatible and fluxing elements to the arc and crustal system. Hydrous basaltic magmas generated by flux melting pond at the crust and mantle boundary and evolve through fractional crystallization and crustal assimilation to felsic parental melts. Progressive crustal metamorphism and anatexis, particularly muscovite, and biotite dehydration melting**,** modifies melt fertility and trace-element signatures. H_2O-rich conditions lower the solidus and enhance Li, Be, Rb, Cs and Ta mobility, whereas comparatively dry, less enriched melts generate barren pegmatites.

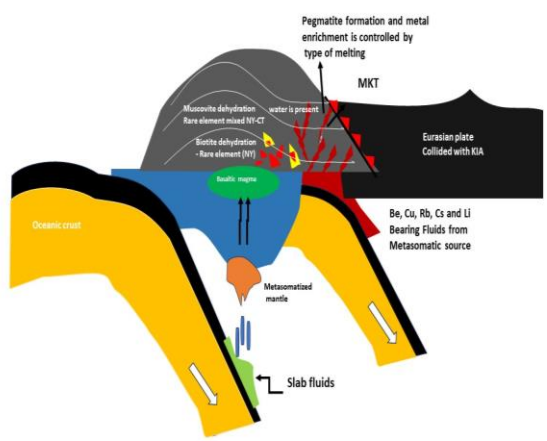

Fig. 11 Subduction collision model for rare-element pegmatite genesis, involving slab-fluid metasomatism, basaltic magmatism, and fluid-present crustal melting (MKT), generating Be, Cu, Rb, Cs and Li-enriched pegmatites during Eurasia and KIA collision.

Early, metal poor melts correspond to barren pegmatites, whereas late residual melts become strongly enriched in incompatible elements and form productive pegmatites. Upward migration along fractures and shear zones facilitates final emplacement and crystallization. Mainly, KLIA pegmatites record a hybrid mantle–crustal system in which source enrichment, volatile fluxing, extreme differentiation, and structural focusing collectively govern rare-metal fertility**.**

Conclusion

The KLIA pegmatites comprise a genetically coherent suite of productive and barren pegmatites generated through variable degrees of magmatic fractionation**.** Productive pegmatites are distinguished by pronounced enrichment in Li, Rb, Cs, Nb, Ta, and Sn, together with elevated Rb/Sr and Cs/Rb and depressed K/Rb and Nb/Ta ratios**,** reflecting advanced differentiation, volatile enrichment, and efficient partitioning of rare elements into late-stage melts. In contrast, barren pegmatites reflect comparatively limited fractionation and weaker rare-element enrichment. Their emplacement along shear zones, fractures, and lithological contacts indicates that structural architecture played a critical role in melt migration, localization, and crystallization. Collectively, the integrated geochemical, mineralogical, and structural criteria provide robust discrimination between productive and barren pegmatites and establish K/Rb, Rb/Sr, Cs/Rb, and Nb/Ta ratios as practical fractionation fertility indicators. These criteria provide effective geochemical and structural vectors for Li, Cs, and Ta exploration within the KLIA and may be applicable to other orogenic and arc-related rare-element pegmatite systems.

Acknowledgement

This study was conducted within an ongoing mineral exploration program in northern Pakistan at Shiraz University. The authors thank SAO International (Pvt.) Ltd., Shees Ahmed Memon, and SGS Pakistan (Pvt.) Ltd. for logistical, field, data, and analytical support.

Statements and Declarations

Funding

This research was funded by SAO International under internal research initiative Grant No. PEG-4-02.

Competing Interests

The authors declare that they have no competing financial or non-financial interests that could have influenced the work reported in this manuscript.

Author Contributions

Johar Ali: conceptualization, methodology, data collection, analysis, and writing. Kamaran Siddique: review and editing. All authors approved the final manuscript.

Data Availability

All data supporting the findings of this study are provided within the manuscript and its supplementary materials.

References

Ahmad, I., Khan, T., Ali, S. and Hussain, M. (2025). Petrogenesis and tectonic evolution of granitoids in the Kohistan-Ladakh Island Arc, northern Pakistan. *J. Asian Earth Sci*., **245**: 105678.

Bachmann, O., and Bergantz, G.W. (2008). The magma reservoirs that feed supereruptions. Elements, **4**(1): 17-21.

Bell, E.A., and Bomgaars, A.W. (2015). Rare-element pegmatites and their exploration significance. *Econ. Geol*., **110**(4): 1025-1042.

Blundy, J., and Wood, B. (2003). Partitioning of trace elements between crystals and melts. *Earth Planet. Sci. Lett*., **210**(3-4): 383-397.

Bowen, N.L. (1928). The evolution of the igneous rocks. Princeton University Press.

Bradley, D.C., McCauley, A.D. and Stillings, L.L. (2017). Mineral-deposit model for lithium–cesium, tantalum (LCT) pegmatites. U.S. Geological Survey Scientific Investigations Report 2010–5070-O, 1-38.

Burg, J.P., Bodinier, J.L., Chaudhry, S., Hussain, S. and Dawood, H. (2006). Kohistan arc: Structure and geodynamic evolution. *Geol. Soc. Am. Bull*., **118**(9-10): 1039-1059.

Cerny, P. (1991). Rare-element granitic pegmatites. Part I: Anatomy and internal evolution of pegmatite deposits. *Geoscience* Canada, **18**(2): 49-67.

Cerny, P. and Ercit, T.S. (2005). The classification of granitic pegmatites revisited. *Can. Mineral*, **43**(6): 2005-2026.

Cerny, P., London, D. and Novak, M. (2012). Granitic pegmatites as reflections of their sources. *Elements*, **8**(4): 289-294.

Chaudhry, M.N., Ghazanfar, M., Ramsay, J.G., Spencer, D.A. and Qayyum, M. (1997). The Higher Himalaya in Pakistan: A tectonostratigraphic synopsis. Geol. Bull. Punjab Univ., **31-32**: 1-22.

Coward, M.P., Jan, M.Q., Rex, D., Tarney, J., Thirlwall, M. and Windley, B.F. (1987). Collision tectonics in the NW Himalayas. *Geological Society*, London, Special Publications, **19**(1): 203-219.

DiPietro, J.A. and Pogue, K.R. (2004). Tectonostratigraphic subdivisions of the Himalaya: A view from the west. *Tectonics*, **23**(5): TC5001.

Gaetani, M., Garzanti, E. and Sciunnach, D. (1990). Evolution of the Karakoram block and its significance for the India-Eurasia collision. *Geodinamica Acta*, **4**(1): 35-49.

Grove, T.L., Till, C.B., Krawczynski, M.J. and Medard, E. (2012). Experimental petrology of mantle melting and magma evolution. Contrib. Mineral. Petrol., **163**(5): 925-948.

Hanson, C. R. (1988). Structure and metamorphism of the

Karakoram gneisses in the Braldu-Shigar region, northern Pakistan. *Geodinamica Acta*, **2**(3-4): 185-202.

Hanson, C.R. (1989). The northern suture in the Shigar Valley, Baltistan, northern Pakistan. *In*: L.L. Malinconico Jr. & R.J. Lillie (Eds.), Tectonics of the Western Himalaya (Geological Society of America Special Paper 232, pp.203-215).

Jagoutz, O. and Behn, M.D. (2013). Foundering of lower island-arc crust as an explanation for the origin of the continental Moho. *Nature*, **504**(7478): 131-134.

Jagoutz, O. and Kelemen, P.B. (2015). Role of arc processes in continental crust formation. Annu. Rev. Earth Planet. Sci., **43**: 363-404.

Jagoutz, O., Muntener, O., Schmidt, M.W. and Burg, J. P. (2007). The roles of flux- and decompression melting in the formation of the Kohistan arc. *Nature,* **448**(7157): 976-979.

Jagoutz, O., Royden, L., Holt, A. F. and Becker, T.W. (2015). Anomalously fast convergence of India and Eurasia caused by double subduction. Nat. Geosci., **8**(6): 475-478.

Kazmi, A. H. and Jan, M. Q. (1997). Geology and tectonics of Pakistan. Graphic Publishers.

Kesler, S.E., Gruber, P.W., Medina, P.A., Keoleian, G.A., Everson, M.P. and Wallington, T.J. (2012). Global lithium resources: Relative importance of pegmatite, brine and other deposits. Ore Geol. Rev., **48**: 55-69.

Khan, M.A., Jan, M.Q., Weaver, B.L. and Windley, B.F. (2009). Evolution of the Kohistan arc: Constraints from geochemistry and geochronology. J. Geol. Soc., **166**(5): 985-999.

Le Fort, P. and Pecher, A. (2002). The Himalayan main central thrust and associated tectono-metamorphic evolution. J. Asian Earth Sci., **20**(4): 459-472.

Linnen, R.L., Van Lichtervelde, M. and Cerny, P. (2012). Granitic pegmatites as sources of strategic metals. *Elements,* **8**(4): 275-280.

London, D. (2008). Pegmatites. Mineralogical Association of Canada.

London, D. (2018). Rare-element granitic pegmatites. *In*: H.D. Holland and K.K. Turekian (Eds.). Treatise on Geochemistry, Elsevier, **13**: 423-456.

London, D. and Morgan, G.B. (2017). The pegmatite puzzles. *Elements*, **13**(6): 399-404.

Molnar, P. and Tapponnier, P. (1975). Cenozoic tectonics of Asia: Effects of a continental collision. *Science*, **189**(4201): 419–426.

Muller, A., Seltmann, R. and Halls, C. (2022). Rare-metal granites and pegmatites: A product of extreme differentiation. *Ore Geol. Rev*., **141**: 104682.

Palin, R.M., Searle, M.P., Waters, D.J., Parrish, R.R., Roberts, N.M.W., Horstwood, M.S.A. and Yeh, M.W. (2018). Early Paleozoic orogenesis in the western Himalaya constrained by U–Pb zircon geochronology. Gondwana Res., **53**: 1-20.

Searle, M.P. and Khan, M.A. (1996). Geological evolution of the Kohistan-Ladakh island arc. J. Geol. Soc., **153**(3): 501-512.

Searle, M.P., Khan, M.A., Fraser, J.E., Gough, S.J. and Jan, M.Q. (2020). The tectonic evolution of the Kohistan-Ladakh island arc. Geol. Soc. Am. Bull., **132**(1-2): 1-24.

Searle, M.P., Windley, B.F., Coward, M.P., Cooper, D.J.W., Rex, D., Li, T., Xiao, X., Jan, M.Q., Thakur, V.C. and Kumar, S. (1999). The closing of the Tethys and the tectonics of the Himalaya. Geol. Soc. Am. Bull., **111**(4): 620-640.

Selway, J.B., Cerny, P. and Breaks, F.W. (2005). Granitic pegmatite-hosted rare-element mineralization: Petrogenesis and exploration. *Economic Geology*, 100th Anniversary Volume, pp.613-635.

Simmons, W.B., Webber, K.L. and Falster, A.U. (2020). Pegmatite genesis and classification: A review. *Minerals*, **10**(9): 812.

Smith, R.L., Johnson, T.E. and Brown, M. (2024). Trace element systematics and fertility indicators in granitic pegmatites. *Lithos*, **450**: 107201.

Tahir-Kheli, R.A.K., Mattauer, M., Proust, F. and Tapponnier, P. (1979). The India-Eurasia suture zone in northern Pakistan: Synthesis and interpretation of recent data at plate scale. Ann. Géol. Himal., **9**: 107-144.

Wadia, D.N. (1931). The syntaxis of the northwest Himalaya: Its rocks, tectonics and orogeny. Geological Survey of India.

Wang, R., Li, J. and Zhang, H. (2023). Geochemical constraints on rare-metal pegmatite formation and evolution. *Ore Geol. Rev*., **156**: 105412.

White, W.M. (2013). Geochemistry. Wiley-Blackwell.

Wilson, M. (1989). Igneous petrogenesis: A global tectonic approach. *Springer*.

Wise, M. A. and Brown, M. (2024). Granite–pegmatite systems and rare-element mineralization. *Elements*, **20**(1): 45-50.

Yin, A. (2006). Cenozoic tectonic evolution of the Himalayan orogen as constrained by a long-strike variation of structural geometry. *Earth-Sci. Rev*., **76**(1-2): 1-131.